44th AIAA Aerospace Sciences Meeting and Exhibit
9 - 12 January 2006, Reno, Nevada

AIAA 2006-370

Automatic Magnetohydrodynamic Control of Hypersonic Flow Using a Discrete Adjoint Formulation

Andre C. Marta*, Juan J. Alonso†
Stanford University, Stanford, CA 94305

Lei Tang‡
ZONA Technology, Inc., Scottsdale, AZ 85251

A significant amount of work in the analysis of high-speed magnetohydrodynamics (MHD) has been carried out during the past decade. However, the fact remains that very little effort has been devoted to design applications of these analysis tools. The main reasons for this lack of design focus have been that the analysis tools were in the process of maturing and that the cost of the simulations was sufficiently large that design applications were beyond the reach of existing computing resources. The absence of such a design framework that provides automated multi-disciplinary optimization (MDO) capabilities for this class of high-speed problems is the principal motivation for this work. This paper develops the foundation of one of the components of such an MDO environment. Control theory has already proved successful in dealing with both aerodynamic shape and aerostructural optimization problems and in this work it is extended to MHD. The discrete adjoint approach emerges as the best suitable option to deal with the complex equations that govern MHD and with the nature of the cost and constraint functions that may be used for relevant design problems. The equations governing the three-dimensional flow of a compressible conducting fluid in a magnetic field using the low magnetic Reynolds number approximation are used. At this stage, other simplifications are assumed, such as a frozen chemical state, so that the soundness of the basic derivations can be established. The details of the theory and implementation of the discrete adjoint solver for the MHD equations are presented in this paper. The gradients obtained using the discrete adjoint approach are validated against finite-difference approximations and shown to be very accurate. A demonstration of the design capabilities is also included with a simple design problem using several design variables and constraints.

I. Introduction

During the last few years, there has been renewed interest in hypersonic flight, leading to an extensive number of conceptual studies.[1] However, it was not until November 2004 that the first successful hypersonic flight of a vehicle with an air-breathing engine was accomplished.[2] It is clear that many technical and scientific obstacles still remain in order to reach the stage where hypersonic flight enters our daily lives.

It is well known that when air flows at hypersonic speeds around blunt bodies, very strong detached shock waves emerge in the regions of intense flow deceleration. There, much of the mean flow kinetic energy is

*Doctoral Candidate, AIAA Member
†Associate Professor, AIAA Member
‡Engineering Specialist, AIAA Member

converted into internal energy, namely translational and vibrational energy, which causes the temperature of the air to increase dramatically. In turn, this temperature increase leads to the dissociation and ionization of the air. Under certain conditions, the air is no longer in thermodynamic equilibrium, as the chemical processes occur in a time scale comparable to the flow time scale. This thermal and chemical non-equilibrium makes the analysis of such flows extremely complex and computationally expensive due to the high stiffness of the chemical equations that need to span several time scales.

In order to cope with the extreme complexity of the full MHD analysis, several simplified models have been developed. The problem can first be approached by ignoring viscous and heat transfer effects. In addition, one can neglect the effects of the electrostatic force and the displacement current and resistivity. With these simplifications, the MHD equations reduce to the ideal MHD formulation.[3]

If chemical reactions are taken into account, then the chemical model of the reacting gas has to be included in the governing equations, which dramatically increases the computational cost. This has been shown in Damevin and Hafmann work,[4] where a complete comparison of the ideal MHD and the Euler solutions, considering frozen, equilibrium and non-equilibrium chemical states has been done. Another good example of the increasingly added accuracy and difficulty in analyzing the flow at hypersonic speeds can be seen from MacCormack's work[5, 6, 7, 8] in which the ideal two-dimensional MHD approach evolved into a three-dimensional method with chemical and thermal non-equilibrium, dealing with both external and internal flows.

To date, accurate models have already been used to predict complex flows, such the one at the scram-jet of an hypersonic vehicle,[9] and there has also been some work done trying to control the flow in scram-jet inlets,[10] but no true effort has come out to automate the control process.

Given that the analysis of MHD flows (with all the appropriate simplifications) has reached a certain level of maturity, it is important that an efficient design framework is built around MHD prediction capabilities, that can be used in multi-disciplinary optimization applications. The control theory approach, also called the adjoint method since the necessary gradients are obtained through the solution of the adjoint equations of the governing equations, emerges as an excellent candidate in achieving that goal.

This theory has been mathematically well documented[11] and the method has already been extensively applied to aerodynamic shape optimization problems governed by the Euler and Navier-Stokes equations using multi-block structured and unstructured meshes in a parallel environment.[12, 13, 14, 15]

The adjoint formulation can be classified into continuous[12] or discrete,[16] depending on whether the formulation is based on the continuous or the discretized form of the governing equations, respectively. There have been some studies comparing these two approaches,[17, 18] but, in principle, none prevails over the other in general, as their relative performance is problem dependent.

However, the continuous adjoint equations for sets of complex governing equations may be impossible to derive without neglecting the variation of parameters such as the viscosity μ and the heat conduction coefficient κ.[18] When considering high-speed flows in the context of MHD, both turbulence and electromagnetic effects play an important role, and the variation of μ and κ, as well as the magnetic permeability μ_m and the electrical conductivity σ, must be taken into account to accurately model the phenomena. Since these variations can be naturally included in the discrete adjoint formulation, this approach seems to be the most suitable for the problem at hand. Moreover, the discrete adjoint formulation can treat arbitrary cost functions and constraints, whereas the continuous adjoint can only treat specific forms of integral functions.[19, 20] The discrete adjoint formulation might be harder to derive (although this can be automated), but it produces more accurate gradients in the sense that they are consistent with the flow solver.

The goal of this work is to extend the discrete adjoint theory to the control of a hypersonic flow in the presence of magnetic fields. Our main objective is to demonstrate the feasibility of this approach with a set of simplified governing equations. The methodology and the design problem formulation have been chosen, however, so that the extension to more complex forms of the governing equations and more realistic design problems can be treated transparently.

In the following sections we describe the various components of the design method that we have created. We start with the description of the physical model, in particular the governing equations of the hypersonic flow under the influence of magnetic fields, and the discrete adjoint formulation. We then provide details of the numerical methods used both for the flow solution and the adjoint solution. Next, a set of sensitivity validation cases involving several types of design variables are shown. These range from a few up to several thousand design variables. A sample design problem is also shown to demonstrate the capabilities of the optimization framework built. Lastly, some remarks are made concerning steps that will by taken in the future in order to achieve a more accurate and capable framework.

II. Physical Model

A. Governing Equations

The equations governing the three-dimensional flow of a compressible conducting fluid in a magnetic field are obtained by coupling the Navier-Stokes equations to the Maxwell equations. Under certain assumptions, this results in a set of equations stating the laws of conservation of mass, momentum and energy, and the evolution of the magnetic induction vector known as the full MHD equations.[21] Several non-dimensional parameters are formed in this formulation, namely the magnetic force number

$$R_b = \frac{B_{ref}^2}{\rho_{ref} U_{ref}^2 \mu_{m_{ref}}}\,, \tag{1}$$

and the magnetic Reynolds number

$$Re_\sigma = \mu_{m_{ref}} \sigma_{ref} U_{ref} L_{ref}\,, \tag{2}$$

in addition to the usual Re, M, etc, parameters found in the equations of fluid flow.

If the environment of interest is characterized by a low magnetic Reynolds number, then the magnetic field induced by the current is much smaller than that imposed on the flow and therefore it can be neglected.[10] This way there is no need to solve the three induction equations in the governing equations and the electromagnetic forces and energy show up as straightforward source terms in the Navier-Stokes equations. Furthermore, if the viscous effects and heat transfer are neglected, the Navier-Stokes equations can be simplified to the so-called Euler equations. In this case, the non-dimensional equations governing the flow are, in conservation form

$$\frac{\partial \mathbf{W}}{\partial t} + \nabla \cdot \vec{\mathcal{F}} = \mathbf{S}\,, \tag{3}$$

where $\mathbf{W}$ is the vector of conservative variables defined as

$$\mathbf{W} = \begin{pmatrix} \rho \\ \rho u \\ \rho v \\ \rho w \\ \rho E \end{pmatrix} \tag{4}$$

and $\vec{\mathcal{F}}$ is the flux vector

$$\vec{\mathcal{F}} = \mathbf{E}\hat{e}_x + \mathbf{F}\hat{e}_y + \mathbf{G}\hat{e}_z\,. \tag{5}$$

The inviscid fluxes **E**, **F** and **G** in the x, y and z directions, respectively, are given by

$$\mathbf{E} = \begin{pmatrix} \rho u \\ \rho u^2 + p \\ \rho uv \\ \rho uw \\ \rho Hu \end{pmatrix}, \quad \mathbf{F} = \begin{pmatrix} \rho v \\ \rho vu \\ \rho v^2 + p \\ \rho vw \\ \rho Hv \end{pmatrix} \quad \text{and} \quad \mathbf{G} = \begin{pmatrix} \rho w \\ \rho wu \\ \rho wv \\ \rho w^2 + p \\ \rho Hw \end{pmatrix}, \tag{6}$$

where ρ is the density, u, v and w are the Cartesian velocity components, p is the static pressure and H is the total enthalpy, which is related to the total energy by $H = E + \frac{p}{\rho}$.

The source term **S** includes the magnetic field terms and is given by

$$\mathbf{S} = \begin{pmatrix} 0 \\ Q\sigma \left[B_z \left(E_y + wB_x - uB_z \right) - B_y \left(E_z + uB_y - vB_x \right) \right] \\ Q\sigma \left[B_x \left(E_z + uB_y - vB_x \right) - B_z \left(E_x + vB_z - wB_y \right) \right] \\ Q\sigma \left[B_y \left(E_x + vB_z - wB_y \right) - B_x \left(E_y + wB_x - uB_z \right) \right] \\ Q\sigma \left[E_x \left(E_x + vB_z - wB_y \right) + E_y \left(E_y + wB_x - uB_z \right) + E_z \left(E_z + uB_y - vB_x \right) \right] \end{pmatrix}, \tag{7}$$

where **B** is the magnetic field, **E** is the electric field, σ is the electrical conductivity and Q is the magnetic interaction parameter defined as

$$Q = \frac{\sigma_{ref} B_{ref}^2 L_{ref}}{\rho_{ref} U_{ref}} = R_b Re_\sigma \,. \tag{8}$$

Integrating (3) over an arbitrary volume Ω and making use of the Gauss' theorem yields

$$\frac{\partial}{\partial t} \int_\Omega \mathbf{W} \mathrm{d}\Omega + \int_{\partial\Omega} \vec{\mathcal{F}} \cdot \mathrm{d}\vec{S} = \int_\Omega \mathbf{S} \, \mathrm{d}\Omega \,, \tag{9}$$

which is the basis for the finite volume numerical discretization.

B. Thermodynamic Model

In this initial work, the gas is assumed to be in thermodynamic equilibrium and to be calorically perfect, thus the equation of state for perfect gases $p = \rho RT$ holds, and the internal energy and the enthalpy relate to the gas temperature by $e = C_v T$ and $h = C_p T$, respectively.

C. Chemical Model

In the present work, the flow is assumed to be frozen, so chemical reactions are neglected. This is done, at this initial stage, so that the soundness of the basic derivations could be established.

III. Adjoint Formulation

The control theory approach has been used extensively both aerodynamic shape optimization and aero-structural design.[12,13,14,16] This approach is well known for its capability to effectively handle design problems involving a large number of design variables and a few objective functions. The sensitivity of the function with respect to an arbitrarily large number of parameters is obtained by solving a system of equations of size equivalent to the governing equations of the flow. When compared to traditional finite-difference methods, the adjoint approach enables large computational savings at the expense of a more complex implementation.[22]

Let $\mathbf{W}$ be the vector of all flow variables at discrete grid points arising from an approximate solution of the governing equations, α the set of design variables which influence the flow, and J the scalar function which approximates the desired cost function. Then, in the context of control theory, the PDE-constrained design problem can be posed as

$$\begin{aligned} Minimize \quad & J(\mathbf{W},\alpha) \\ w.r.t \quad & \alpha \\ subject\ to \quad & \mathbf{R}(\mathbf{W},\alpha) = 0\,, \end{aligned} \tag{10}$$

where $\mathbf{R}(\mathbf{W},\alpha) = 0$ represents the discrete flow equations and boundary conditions that must be satisfied.

The sensitivity of the cost function with respect to the design variables is required to solve the problem using gradient-based optimization algorithms such as, for example, sequential quadratic programing (SQP).

Following the method of Lagrange multipliers for the solution of a constrained minimization problem, the augmented cost function is defined as

$$I(\mathbf{W},\alpha) = J(\mathbf{W},\alpha) - \lambda^T \mathbf{R}(\mathbf{W},\alpha)\,, \tag{11}$$

where λ is the vector of Lagrange multipliers, also called adjoint variables. From the definition of augmented cost function, the constraints are naturally enforced by the optimal solution, thus the governing equations are automatically satisfied. The sensitivity of the augmented cost function (11) is then

$$\frac{dI}{d\alpha} = \frac{dJ}{d\alpha} - \lambda^T \frac{dR}{d\alpha}\,, \tag{12}$$

which can be expanded as

$$\frac{dI}{d\alpha} = \left(\frac{\partial J}{\partial W}\frac{dW}{d\alpha} + \frac{\partial J}{\partial \alpha}\right) - \lambda^T \left(\frac{\partial R}{\partial W}\frac{dW}{d\alpha} + \frac{\partial R}{\partial \alpha}\right)\,. \tag{13}$$

Rearranging equation (13) results in

$$\frac{dI}{d\alpha} = \left(\frac{\partial J}{\partial W} - \lambda^T \frac{\partial R}{\partial W}\right)\frac{dW}{d\alpha} + \left(\frac{\partial J}{\partial \alpha} - \lambda^T \frac{\partial R}{\partial \alpha}\right)\,. \tag{14}$$

In order to eliminate the dependence on the flow variables, the term involving $dW/d\alpha$ must vanish, which is achieved by choosing λ such that it satisfies the adjoint equation

$$\frac{\partial J}{\partial W} - \lambda^T \frac{\partial R}{\partial W} = 0 \qquad \Longrightarrow \qquad \left[\frac{\partial R}{\partial W}\right]^T \lambda = \left[\frac{\partial J}{\partial W}\right]^T\,. \tag{15}$$

Once λ is obtained by solving the system of equations (15), the sensitivity of the augmented cost function is simply given by

$$\frac{dI}{d\alpha} = \frac{\partial J}{\partial \alpha} - \lambda^T \frac{\partial R}{\partial \alpha}\,. \tag{16}$$

This sensitivity can then be used to find the search direction of the gradient based optimization algorithm as indicated in figure 1.

The advantage of the adjoint approach can be seen from equation (16), which is independent of $\delta\mathbf{W}$, meaning that the gradient of I with respect to an arbitrary large vector of design variables α can be determined without the need for additional flow-field evaluations.

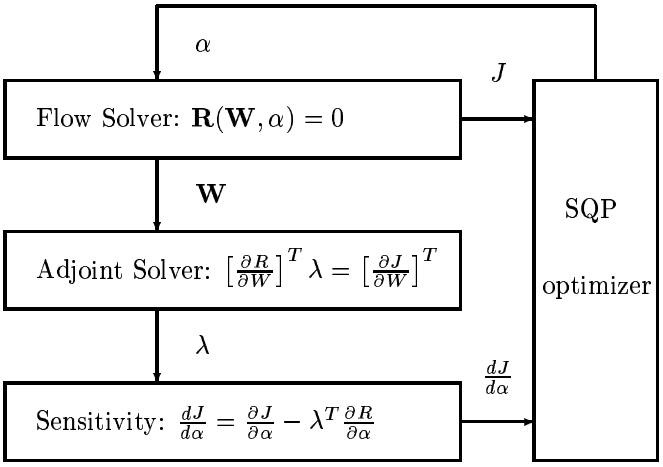

Figure 1. Schematic of the Adjoint-Based Optimization Algorithm.

If the design problem (10) includes m additional constraints to the governing equations, such as aerodynamic or magnetic constraints, function of the flow solution $\mathbf{W}$ and the design variables α,

$$C_i(\mathbf{W}, \alpha) = 0 \qquad i = 1, ..., m\,, \tag{17}$$

where C_i is a scalar function, then the use of a gradient based algorithm also requires information about their sensitivities, which in turn implies another m adjoint calculations.

IV. Numerical Model

A. MHD Solver

Several discretization schemes have been applied to hypersonic flows, ranging from explicit flux splitting schemes such as Roe, Van Leer and Steger-Warming,[23,24] as well as implicit schemes, using approximate factorization procedures[25] and higher-order compact schemes.[21] For the present work, the Jameson-Schmidt-Turkel (JST) explicit scheme[26] is used. This scheme uses an artificial dissipation term, which is a blend of first- and third-order-accurate terms to provide good numerical stability properties while keeping its implementation relatively easy and computationally inexpensive.

A cell-centered finite volume spacial discretization scheme is applied on a body-fitted structured mesh of hexahedral cells. The scheme reduces to a central difference scheme on a Cartesian grid and is second-order accurate provided that the mesh is sufficiently smooth.

A set of coupled ordinary differential equations (ODEs) is then obtained by applying equation (9) separately to each computational cell and since the cell volume V_{ijk} is independent of time, it can be rewritten in the form

$$\frac{d\mathbf{W}_{ijk}}{dt} + \mathbf{R}(\mathbf{W})_{ijk} = 0\,, \tag{18}$$

where $\mathbf{W}$ is the vector of the flow variables at the cell centers, and $\mathbf{R(W)}$ is the vector of the residuals. The residual

$$R_{ijk} = \frac{1}{V_{ijk}}(Q_{ijk} - D_{ijk} - M_{ijk}) \tag{19}$$

consists of the inviscid flux terms Q_{ijk}, together with the scalar artificial dissipation terms D_{ijk} and the magnetic source terms M_{ijk}, defined by the space discretization scheme as shown in figure 2.

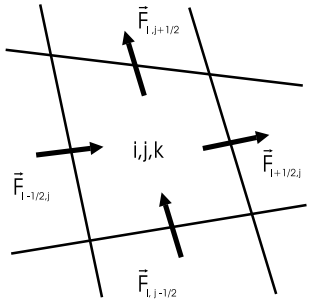

Figure 2. Fluxes.

Since the primary objective is to obtain a steady-state solution, the time marching scheme was selected for its simplicity, stability and damping properties. Therefore, an explicit five-stage modified Runge-Kutta scheme was used to integrate (18) in time, using the coefficient values were obtained from reference.[27] In addition, adaptive local time step[28] is used to increase the convergence rate of the algorithm.

Using a body conforming mesh, the boundary condition implementation becomes greatly simplified. Inflow and outflow are trivially imposed at hypersonic boundaries, as all the characteristics of the governing equations (3) travel downstream. As such, the complete vector of conservation variables is fixed at the supersonic incoming boundary, whereas the values at the supersonic outflow boundary are extrapolated from the interior. As for the solid boundary defining the body surface, according to the impermeability condition, the velocity vectors at the halo cells are set in such a way that the normal fluxes at the boundary are zero and the pressure is linearly extrapolated from the interior cells.

B. Discrete Adjoint Formulation

The big conceptual difference between the continuous adjoint and the discrete adjoint is that the latter uses the algebraic equations that result from the discretization of the governing equations, as opposed to the continuous approach that formulates the adjoint equations from the continuous governing equations, and only then discretizes them.

As such, the discrete adjoint system of equations (15) is constructed by differentiating all the numerical fluxes that comprise the residual R_{ijk} (19) of the discretized governing equations with respect to the flow variables themselves. Because the residual applies to every computational cell, it follows that the matrix $\frac{\partial R}{\partial W}$ of the adjoint system of equations has dimensions $(nic \times nfv)^2$, where nic is the number of internal cells and nfv the number of flow variables.

Since a structured computational mesh is used, the result is multi-diagonal matrix, whose entries are block matrices of dimension nfv^2, making the global matrix very sparse and thus easily stored. The number of non-zero diagonals matches the dimension of the stencil used in the flow solver. For the present 3-D spatial discretization, a stencil with thirteen cells is used.

Even though a full three-dimensional adjoint solver was developed, a 1-dimensional case is shown here for illustration purposes. The block matrices entries of the global adjoint matrix $\frac{\partial R}{\partial W}$ for cell i are computed as

$$\mathcal{D}_i(m,n) = \frac{\partial R_i(m)}{\partial W_{i-2}(n)}\,, \quad \mathcal{B}_i(m,n) = \tfrac{\partial R_i(m)}{\partial W_{i-1}(n)}\,, \quad \mathcal{A}_i(m,n) = \frac{\partial R_i(m)}{\partial W_i(n)}$$
$$\mathcal{C}_i(m,n) = \frac{\partial R_i(m)}{\partial W_{i+1}(n)}\,, \quad \mathcal{E}_i(m,n) = \tfrac{\partial R_i(m)}{\partial W_{i+2}(n)}\,. \tag{20}$$

Recalling the different residual contributions expressed in equation (19), the adjoint matrix can be assembled by adding up the contributions of each term.

The inviscid terms are due to the flux through both the west and east cell faces $Q_i = Q_{i+1/2} - Q_{i-1/2}$. Considering the $i+1/2$ face, the flux

$$Q_{i+1/2} = \left(\vec{\mathcal{F}}\cdot\vec{S}\right)_{i+\frac{1}{2}} = \frac{1}{2}\left(\vec{\mathcal{F}}_{i+1}\cdot\vec{S}_i + \vec{\mathcal{F}}_i\cdot\vec{S}_i\right)\,, \quad \text{where} \quad \vec{\mathcal{F}}_i\cdot\vec{S}_i = E_i Sx_i + F_i Sy_i + G_i Sz_i\,,$$

contributes to the adjoint matrix as

$$\mathcal{A}_i = \frac{\partial Q_{i+1/2}}{\partial W_i} = \frac{1}{2}\left(\frac{\partial E_i}{\partial W_i}Sx_i + \frac{\partial F_i}{\partial W_i}Sy_i + \frac{\partial G_i}{\partial W_i}Sz_i\right)\,, \tag{21}$$
$$\mathcal{C}_i = \frac{\partial Q_{i+1/2}}{\partial W_{i+1}} = \frac{1}{2}\left(\frac{\partial E_{i+1}}{\partial W_{i+1}}Sx_i + \frac{\partial F_{i+1}}{\partial W_{i+1}}Sy_i + \frac{\partial G_{i+1}}{\partial W_{i+1}}Sz_i\right)\,. \tag{22}$$

Similarly, the JST[26] artificial dissipation flux through the $i+1/2$ face, given by

$$\begin{aligned} D_{i+\frac{1}{2}} &= \lambda_{i+\frac{1}{2}}\left(\varepsilon^{(2)}_{i+\frac{1}{2}}\Delta_F W_i + \varepsilon^{(4)}_{i+\frac{1}{2}}\Delta_F\Delta_B\Delta_F W_i\right) \\ &= \lambda_{i+\frac{1}{2}}\left[\varepsilon^{(2)}_{i+\frac{1}{2}}(W_{i+1}-W_i) + \varepsilon^{(4)}_{i+\frac{1}{2}}(W_{i+2}-3W_{i+1}+3W_i-W_{i-1})\right]\,, \end{aligned}$$

contributes to the adjoint matrix as

$$\mathcal{B}_i = \frac{\partial D_{i+1/2}}{\partial W_{i-1}} = \lambda_{i+\frac{1}{2}}\left(\frac{\partial \varepsilon^{(2)}_{i+\frac{1}{2}}}{\partial W_{i-1}}\Delta_F W_i + \frac{\partial \varepsilon^{(4)}_{i+\frac{1}{2}}}{\partial W_{i-1}}\Delta_F\Delta_B\Delta_F W_i - \varepsilon^{(4)}_{i+\frac{1}{2}}\right)\,, \tag{23}$$
$$\mathcal{A}_i = \frac{\partial D_{i+1/2}}{\partial W_i} = \lambda_{i+\frac{1}{2}}\left(\frac{\partial \varepsilon^{(2)}_{i+\frac{1}{2}}}{\partial W_i}\Delta_F W_i - \varepsilon^{(2)}_{i+\frac{1}{2}} + \frac{\partial \varepsilon^{(4)}_{i+\frac{1}{2}}}{\partial W_i}\Delta_F\Delta_B\Delta_F W_i + 3\varepsilon^{(4)}_{i+\frac{1}{2}}\right)\,, \tag{24}$$
$$\mathcal{C}_i = \frac{\partial D_{i+1/2}}{\partial W_{i+1}} = \lambda_{i+\frac{1}{2}}\left(\frac{\partial \varepsilon^{(2)}_{i+\frac{1}{2}}}{\partial W_{i+1}}\Delta_F W_i + \varepsilon^{(2)}_{i+\frac{1}{2}} + \frac{\partial \varepsilon^{(4)}_{i+\frac{1}{2}}}{\partial W_{i+1}}\Delta_F\Delta_B\Delta_F W_i - 3\varepsilon^{(4)}_{i+\frac{1}{2}}\right)\,, \tag{25}$$
$$\mathcal{E}_i = \frac{\partial D_{i+1/2}}{\partial W_{i+2}} = \lambda_{i+\frac{1}{2}}\left(\frac{\partial \varepsilon^{(2)}_{i+\frac{1}{2}}}{\partial W_{i+2}}\Delta_F W_i + \frac{\partial \varepsilon^{(4)}_{i+\frac{1}{2}}}{\partial W_{i+2}}\Delta_F\Delta_B\Delta_F W_i + \varepsilon^{(4)}_{i+\frac{1}{2}}\right)\,, \tag{26}$$

neglecting the dependence of the spectral radius $\lambda_{i+\frac{1}{2}}$ on $\mathbf{W}$.

Similar expressions are obtained for the fluxes through all the other cell faces.

As for the magnetic field contribution M_i to the adjoint system, as it is only a volume and not a flux term, it only contributes to

$$\mathcal{A}_i = \frac{\partial M_i}{\partial W_i}\,. \tag{27}$$

So far, only the left-hand side of the adjoint system of equations (15) has been considered. In order to obtain the right-hand side, a cost function J has to be defined and its partial derivative with respect to the conservative variables $\mathbf{W}$ has to be computed. Since the cost function is problem-dependent, several functions may arise. For the present work, both the drag and lift coefficients were considered. The derivation for the former is shown here as an illustration. From the definition of pressure (inviscid) drag coefficient

$$C_D = \frac{1}{q_\infty S_{ref}} \iint_S p_w \hat{n}_D \cdot d\vec{S}\,, \tag{28}$$

where $-\vec{n}_D$ is the direction of the flow, q_∞ is the dynamic pressure, p_w the wall pressure and S_{ref} the reference area. Its discretization in the computational domain, assuming that the body surface occurs at $i = 1$, can be expressed as

$$C_D = \frac{1}{q_\infty S_{ref}} \sum_j \sum_k p_{w_{jk}}\, \hat{n}_D \cdot \vec{S}_{w_{jk}}\,, \tag{29}$$

where $\vec{S}_{w_{jk}}$ is the body surface area of the $(1, j, k)$ cell.

Using the drag coefficient (29) as the cost function, its sensitivity with respect to the conservative variables can then be easily computed as

$$\frac{\partial J}{\partial W} = \frac{\partial C_D}{\partial W} = \frac{1}{q_\infty S_{ref}} \sum_j \sum_k \frac{\partial p_{w_{jk}}}{\partial W} \hat{n}_D \cdot \vec{S}_{w_{jk}}\,. \tag{30}$$

The pressure at the wall p_w is computed using the same boundary condition method as in the flow solver to ensure consistency. If p_w is computed using a linear extrapolation approximation, then $p_w = f(p_2, p_3)$. Consequently, the only nonzero terms are $i = 2$ and $i = 3$, which are given by

$$\frac{\partial J}{\partial W_{i=2}} = \frac{1}{q_\infty S_{ref}} \frac{3}{2} \frac{\partial p_2}{\partial W_2} \hat{n}_D \cdot \vec{S}_w \quad \text{and} \quad \frac{\partial J}{\partial W_{i=3}} = -\frac{1}{q_\infty S_{ref}} \frac{1}{2} \frac{\partial p_3}{\partial W_3} \hat{n}_D \cdot \vec{S}_w\,. \tag{31}$$

This discrete adjoint formulation allows any cost function to be treated in a similar same fashion, independently of its form (unlike the continuous adjoint formulation).

Special care is given at the boundaries, where the cells have stencils that extend outside the internal computational domain, making necessary modifications according to the corresponding boundary condition method used in the flow solver. This happens because the adjoint system is only solved for the interior cells and so all the exterior boundary cell values have to be written as functions of the interior domain.

Given the adjoint matrix entries (20) and right-hand side entries (30), the discrete adjoint system of equations is assembled as shown in equation (32).

$$\begin{bmatrix} & & & & & & & & & & \\ \cdots & \ddots & \ddots & \ddots & \ddots & \ddots & 0 & 0 & 0 & 0 & \cdots \\ \cdots & 0 & \mathcal{D}_{i-1} & \mathcal{B}_{i-1} & \mathcal{A}_{i-1} & \mathcal{C}_{i-1} & \mathcal{E}_{i-1} & 0 & 0 & 0 & \cdots \\ \cdots & 0 & 0 & \mathcal{D}_i & \mathcal{B}_i & \mathcal{A}_i & \mathcal{C}_i & \mathcal{E}_i & 0 & 0 & \cdots \\ \cdots & 0 & 0 & 0 & \mathcal{D}_{i+1} & \mathcal{B}_{i+1} & \mathcal{A}_{i+1} & \mathcal{C}_{i+1} & \mathcal{E}_{i+1} & 0 & \cdots \\ & & & & & & & & & & \\ \cdots & 0 & 0 & 0 & 0 & \ddots & \ddots & \ddots & \ddots & \ddots & \cdots \end{bmatrix}^T \begin{bmatrix} \vdots \\ \lambda_{i-2} \\ \lambda_{i-1} \\ \lambda_i \\ \lambda_{i+1} \\ \lambda_{i+2} \\ \vdots \end{bmatrix} = \begin{bmatrix} \vdots \\ \partial J/\partial W_{i-2} \\ \partial J/\partial W_{i-1} \\ \partial J/\partial W_i \\ \partial J/\partial W_{i+1} \\ \partial J/\partial W_{i+2} \\ \vdots \end{bmatrix} \tag{32}$$

In order to solve the large sparse matrix problem (32), the Portable, Extensible Toolkit for Scientific Computation (PETSc)[29,30] is used. Due to the structure of the matrix to be solved, a sparse storage is selected and the system is solved using the Generalized Minimal Residual (GMRES) method in conjunction with an incomplete LU factorization preconditioner.

Once the adjoint solution is found, the gradient of the function of interest is obtained from (16). The terms $\frac{\partial J}{\partial \alpha}$ and $\frac{\partial R}{\partial \alpha}$ are approximated using finite-differences, but being partial derivatives, they are very cheap to compute since no flow re-evaluation is necessary.

C. Gradient-Based Optimizer

The optimization problem is solved by feeding the cost and constraint function values, obtained by the MHD solver, and their gradients, obtained by the adjoint solver, into a gradient-based optimizer. The optimizer used in this work is SNOPT,[31,32] which is a software package for solving large-scale optimization problems (linear and nonlinear programs).

V. Blunt Body Configuration

The configuration used as a preliminary test case follows.[33] The body is a blunt cylinder immersed in a hypersonic incoming flow, at an arbitrary angle of attack and side-slip angle.

A. Magnetic Field

A collection of hypothetical electric circuits is placed inside the body which imposes a magnetic field on the flow. Each elementary circuit is thought to produce a dipole-like magnetic field given by

$$\mathbf{B} = \frac{\mu_0 m}{4\pi r^3} \left[2\cos\theta \hat{e}_r + \sin\theta \hat{e}_\theta \right], \tag{33}$$

where r and θ define the dipole orientation and m is the dipole strength.

It is important to guarantee that the imposed magnetic field satisfies the magnetic field equations, especially if a low magnetic Reynolds number approximation is used. Since the imposed field is obtained from a collection of dipoles, the condition $\nabla \cdot \mathbf{B} = 0$ is automatically satisfied.

B. Body Shape

A collection of bumps is located on the body nose so that shape control can be performed. These bumps are given by Hicks-Henne functions,[34] whose amplitude can be changed during the design process, and are superimposed to the baseline nose radius. This leads to ring-type shape perturbations on the nose surface. The bumps are equally distributed between the nose tip and the 45 degree angular location (with respect to the body axis) and their location is fixed.

VI. Results

A. Effect of the Magnetic Field

The low magnetic Reynolds number MHD solver was validated by running a simulation of a hypersonic flow over a blunt cylinder, similar to the one found in the literature.[33] An incoming flow at Mach=5 aligned with the body axis was used, and a single dipole was located inside the body at the nose center point, also aligned with body axis. Different magnetic field strengths were tested, ranging from $Q = 0$ to $Q = 6$.

The effect on the shock stand-off distance can be seen in figure 3. Being a simple MHD model, and being impossible to compare the values of the non-dimensional parameter directly, one can only argue that the

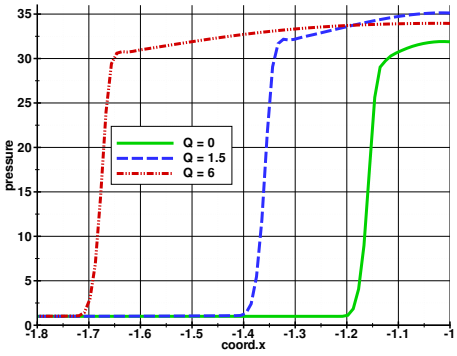

Figure 3. Stand-Off Distance at M=5.

values follow the expected qualitative trend. From table 1, it can be seen that the aerodynamic coefficients vary nonlinearly with the magnetic field. For weak magnetic fields, the drag increases with increasing Q_{mip}, but for stronger fields, it decreases, becoming even smaller than the non-magnetic reference case.

Q_{mip}	C_D	C_L
0	0.8542	0
1.5	0.8782	0
6.0	0.7912	0

Table 1. Aerodynamic Coefficients for Different Magnetic Interaction Parameters.

B. Sensitivity Verification

A validation study of the sensitivities obtained from the discrete adjoint formulation was performed with finite-difference approximations computed using the MHD flow solver.

The results in figure 4 show the drag coefficient sensitivity with respect to the electrical conductivity σ on the body surface and mid plane locations. The mesh size used was 18x16x24, with a single dipole located at the body nose center and oriented against a Mach 5 incoming flow at an angle of attack of 26.6 degrees. The electrical conductivity was assumed to be a design variable in each computational cell, leading to a total of 6912 design variables.

The results obtained using the discrete adjoint approach were matched against values obtained using a finite-difference solution at three control cells located on the body surface (and shown on figure 4 with the dots) and the results are summarized in table 2. The agreement is remarkably good and highlights the potential of the adjoint procedure to be used in problems with a large number of design variables.

Figures 5 and 6 show the drag and the lift coefficient sensitivities with respect to some other design variables. In these cases, the mesh size was 32x48x64, two dipoles were located inside the body, oriented against a Mach 5 incoming flow at an angle of attack of 10 degrees and side-slip angle of 5 degrees. A total of 18 design variables were considered - angle of attack, side-slip angle, bump amplitudes (10 in total) and dipole strengths (2) and orientations (4). The sensitivity computed from the adjoint solution was also compared against a finite-difference approach.

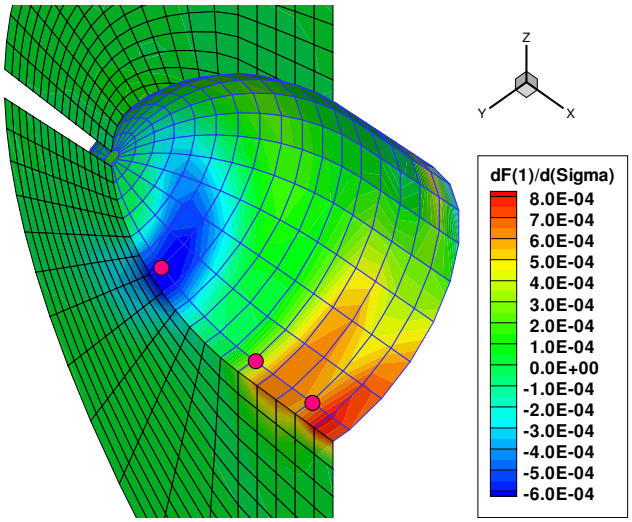

Figure 4. Drag Coefficient Sensitivity with respect to Electrical Conductivity σ.

Cell index (i,j,k)	Adjoint	Finite-Differences	Difference
(8,2,19)	-6.6314E-4	-6.5840E-4	0.72 %
(14,2,19)	2.9937E-4	2.9319E-4	2.11 %
(17,2,19)	5.8642E-4	5.8650E-4	-0.01 %

Table 2. Electrical Conductivity Sensitivity Verification.

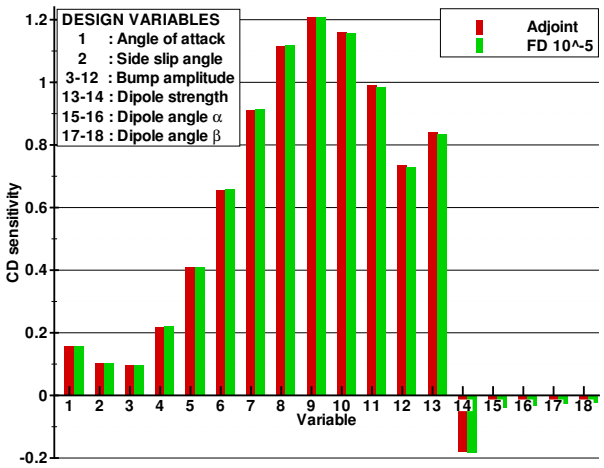

Figure 5. Drag Coefficient Sensitivity.

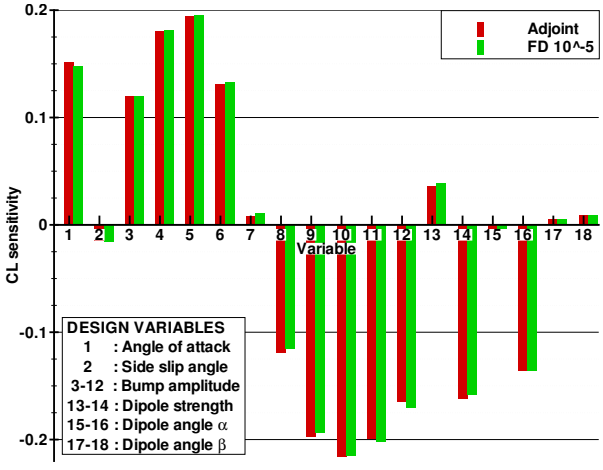

Figure 6. Lift Coefficient Sensitivity.

Once again, there is good agreement, with values within 1.5% for the drag coefficient sensitivity and 3% for the lift coefficient sensitivity.

C. Sample Design Problem

To demonstrate the design capabilities achieved by using the sensitivity information efficiently obtained by the discrete adjoint approach, a simple design problem was solved.

The same blunt body was used, modeling the nose of a re-entry vehicle in the atmosphere. The design problem intends to maximize the drag coefficient, while keeping the lift coefficient in a specified range ($0.04 < C_L < 0.05$).

A total of 21 design variables were used, representing three types of design variables as follows:

- Free-stream direction - angle of attack and side slip angle;
- Shape design variables - 4 Hicks-Henne bumps distributed on the body surface;
- Magnetic field characteristics - strength and orientation of 5 dipoles distributed inside the body, as shown in figure 7.

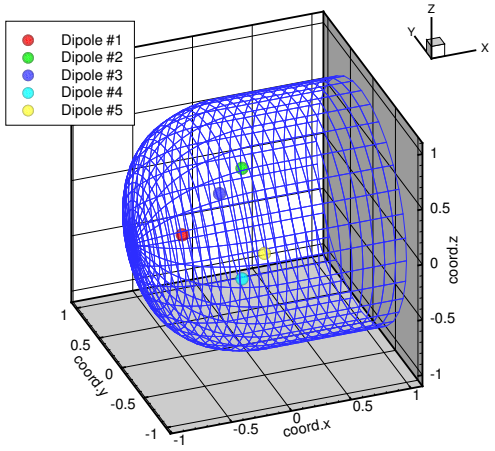

Figure 7. Dipole Locations.

In addition, a design was also done without the dipoles to investigate the importance and impact of the latter in the problem solution. Figure 8 shows the convergence history of the design iterations for both the case with and without dipoles. The initial optimization iterations employ primarily the free-stream and shape design variables, but subsequent iterations perform a fine tuning of the dipole characteristics, which result in a 2.5% improvement over the non-magnetic optimum solution. The optimal dipole strengths were limited by their upper bound of m corresponding to $B_{ref} = 0.06\,T = 600\,Gauss$.

Although the magnetic field imposed by the dipoles is weak, the pressure distribution on the surface body changes significantly compared to the non-magnetic solution. Figure 9 shows this distribution along the body centerline, in which the increase of pressure on both the upper and lower surfaces is the cause of the optimal solution shown in figure 8.

It is interesting also to point out that, even though the shock stand-off distance change is barely noticeable, the overall pressure distribution on the body surface changes considerably, with the pressure recovery from the stagnation point taking longer to occur, as seen in figure 10.

The optimal magnetic field found is shown in figure 11, where a contour of its strength and its vector field are illustrated on the body surface and the center plane.

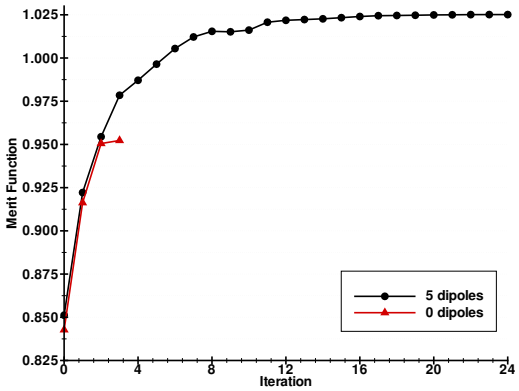

Figure 8. Convergence History of the Design Iterations.

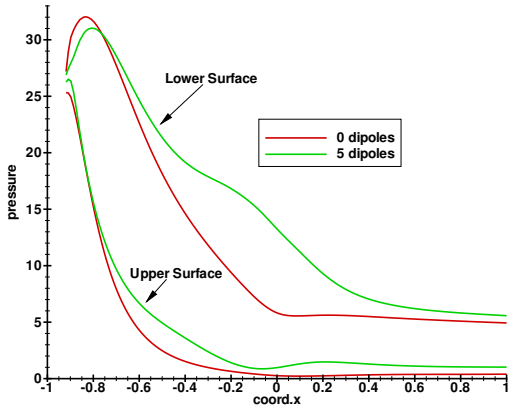

Figure 9. Pressure Distribution Along Centerline.

VII. Conclusions

In this paper we have presented an effective method for large-scale design problems involving high-speed MHD flows.

We have constructed a proof-of-concept methodology that can be extended to treat more complex MHD governing equations and more complex design problems and geometries. The discrete adjoint is the correct approach to follow because of these advantages:

- Well defined procedure to derive adjoint equations **independently** of the complexity of the governing equations;
- Ability to treat **arbitrary** cost functions and constraints (unlike continuous formulation that can only deal with certain classes of integral functions).

The accuracy of the sensitivity of the cost functions of interest to variations of shape, orientation, electrical conductivity and magnetic field strength and orientation was demonstrated to within 1-2%. In addition, the design capabilities have been illustrated with a preliminary application.

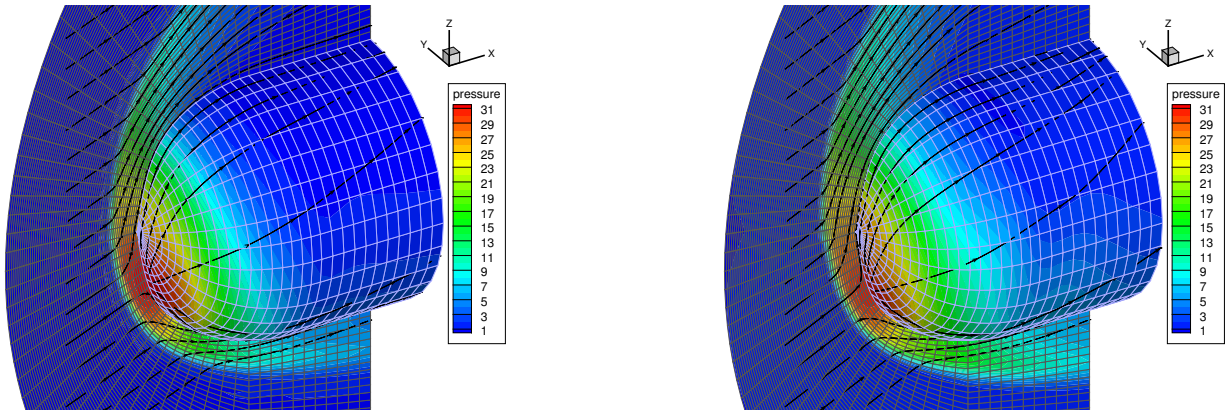

(a) without dipoles

(b) with 5 dipoles

Figure 10. Pressure Distribution.

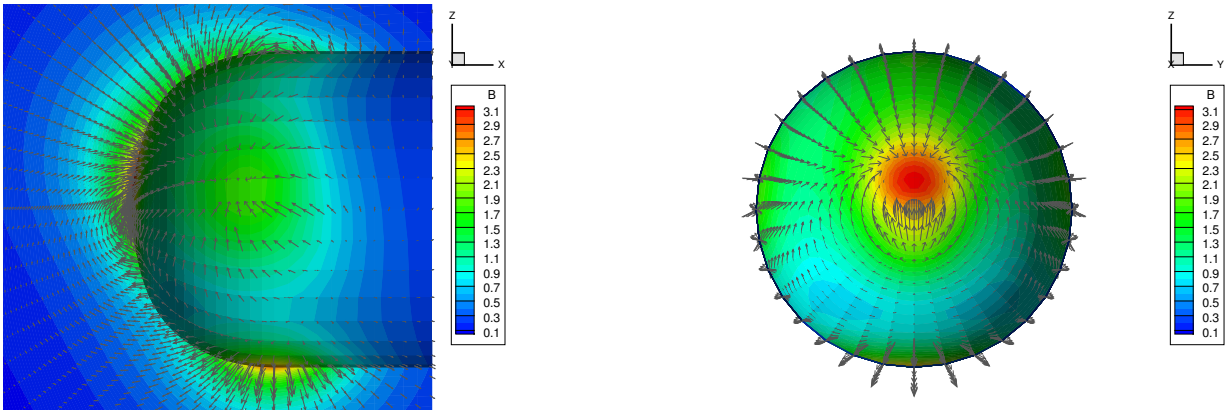

(a) side view

(b) front view

Figure 11. Magnetic Field.

This work represents the first step toward an automatic design framework for problems involving hypersonic flow control using electromagnetic effects. Future work includes the incorporation of the viscous Navier-Stokes terms and the magnetic induction equations in the governing equations, corresponding to the full MHD formulation. Once the flow analysis is extended, the discrete adjoint solver will be adapted accordingly. Besides the derivation of the discrete adjoint equations, the investigation of meaningful design problems and the definition of significant cost functions will also be tackled.

VIII. Acknowledgments

The authors are grateful for Air Force Office of Scientific Research contract No. FA9550-04-C-0105 under tasks monitored by Jonathan Poggie and John Schmisseur. The first author also acknowledges the support of the Fundação para a Ciência e a Tecnologia from Portugal.

References

[1]Hallion, R. P., "The History of Hypersonics: or, Back to the Future – Again and Again," *AIAA Paper* 2005-0329, Jan. 2005, Proceedings of the 43^{rd} AIAA Aerospace Sciences Meeting and Exhibit, Reno, NV.

[2]NASA, "X-43A Hypersonic Scramjet-Powered Research Aircraft," www.nasa.gov/missions/research/x43-main.html.

[3]Augustinus, J., Hoffmann, K. A., and Harada, S., "Numerical Solutions of Ideal MHD Equations for a Symmetric Blunt Body at Hypersonic Speeds," *AIAA Paper* 1998-0850, Jan. 1998, Proceedings of the 36^{th} AIAA Aerospace Sciences Meeting and Exhibit, Reno, NV.

[4]Damevin, H.-M. and Hoffmann, K. A., "Numerical Magnetogasdynamics Simulations of Hypersonic, Chemically Reacting Flows," *AIAA Paper* 2001-2746, June 2001, Proceedings of the 32^{nd} AIAA Plasmadynamics and Lasers Conference, Anaheim, CA.

[5]MacCormack, R. W., "An Upwind Conservation Form Method for Magnetofluid Dynamics," *AIAA Paper* 1999-3609, June 1999, Proceedings of the 30^{th} AIAA Plasmadynamics and Lasers Conference, Norfolk, VA.

[6]MacCormack, R. W., "A Computational Method for Magnetofluid Dynamics," *AIAA Paper* 2001-2735, June 2001, Proceedings of the 32^{nd} AIAA Plasmadynamics and Lasers Conference, Anaheim, CA.

[7]MacCormack, R. W., "Conservation Form Method for Magnetofluid Dynamics," *AIAA Paper* 2001-0195, Jan. 2001, Proceedings of the 39^{th} AIAA Aerospace Sciences Meeting and Exhibit, Reno, NV.

[8]MacCormack, R. W., "Three Dimensional Magneto-Fluid Dynamics Algorithm Development," *AIAA Paper* 2002-0197, Jan. 2002, Proceedings of the 40^{th} AIAA Aerospace Sciences Meeting and Exhibit, Reno, NV.

[9]Deb, P. and Agarwal, R. K., "A Performance Study of MHD-bypass Scramjet Inlets with Chemical Nonequilibrium," *AIAA Paper* 2001-2872, June 2001, Proceedings of the 32^{nd} AIAA Plasmadynamics and Lasers Conference, Anaheim, CA.

[10]Gaitonde, D. V., "Simulation of Local and Global High-Speed Flow Control with Magnetic Fields," *AIAA Paper* 2005-0560, Jan. 2005, Proceedings of the 43^{rd} AIAA Aerospace Sciences Meeting and Exhibit, Reno, NV.

[11]Giles, M. B. and Pierce, N. A., "An Introduction to the Adjoint Approach to Design," *Flow, Turbulence and Combustion*, Vol. 65, Kluwer Academic Publishers, 2000, pp. 393–415.

[12]Reuther, J. J., Jameson, A., Alonso, J. J., Rimlinger, M. J., and Saunders, D., "Constrained Multipoint Aerodynamic Shape Optimization Using an Adjoint Formulation and Parallel Computers, Part 1," *Journal of Aircraft*, Vol. 36, No. 1, 1999, pp. 51–60.

[13]Reuther, J. J., Jameson, A., Alonso, J. J., Rimlinger, M. J., and Saunders, D., "Constrained Multipoint Aerodynamic Shape Optimization Usinf an Adjoint Formulation and Parallel Computers, Part 2," *Journal of Aircraft*, Vol. 36, No. 1, 1999, pp. 61–74.

[14]Kim, H.-J. and Nakahashi, K., "Discrete Adjoint Method for Unstructured Navier-Stokes Solver," *AIAA Paper* 2005-0449, Jan. 2005, Proceedings of the 43^{rd} AIAA Aerospace Sciences Meeting and Exhibit, Reno, NV.

[15]Jameson, A., Sriram, and Martinelli, L., "Aerodynamic Shape Optimization of Transonic and Supersonic Aircraft Configurations," *AIAA Paper* 2005-1013, Jan. 2005, Proceedings of the 43^{rd} AIAA Aerospace Sciences Meeting and Exhibit, Reno, NV.

[16]Nielsen, E. J. and Park, M. A., "Using an Adjoint Approach to Eliminate Mesh Sensitivities in Computational Design," *AIAA Paper* 2005-0491, Jan. 2005, Proceedings of the 43^{rd} AIAA Aerospace Sciences Meeting and Exhibit, Reno, NV.

[17]Nadarajah, S. K. and Jameson, A., "A Comparison of the Constinuous and Discrete Adjoint Approach to Automatic Aerodynamic Optimization," *AIAA Paper* 2000-0667, Jan. 2000, Proceedings of the 38^{th} AIAA Aerospace Sciences Meeting and Exhibit, Reno, NV.

[18]Nadarajah, S. K. and Jameson, A., "Studies of the Continuous and Discrete Adjoint Approaches to Viscous Automatic Aerodynamic Shape Optimization," *AIAA Paper* 2001-2530, June 2001, Proceedings of the 15^{th} AIAA Computational Fluid Dynamics Conference, Anaheim, CA.

[19]Jameson, A., Pierce, N. A., and Martinelli, L., "Optimum Aerodynamic Design using the Navier Stokes Equations," *Theoretical and Computational Fluid Dynamics*, Vol. 10, Springer-Verlag GmbH, Jan. 1998, pp. 213–237.

[20]Lewis, R. M., "Numerical Computation of Sensitivities and the Adjoint Approach," *Computational Methods for Optimal Design and Control*, edited by J. Borggaard, J. Burns, E. Cliff, and S. Schreck, Birkhäuser, 1998, pp. 285–302, Also available as ICASE technical report 97–61.

[21]Gaitonde, D. V., "Higher-Order Solution Procedure for Three-Dimensional Nonideal Magnetogasdynamics," *AIAA Journal*, Vol. 39, No. 11, Nov. 2001, pp. 2111–2120.

[22]Martins, J. R. R. A., Alonso, J. J., and Reuther, J. J., "Complete Configuration Aero-Structural Optimization Using a Coupled Sensitivity Analysis Method," *AIAA Paper* 2002-5402, Sept. 2002, Proceedings of the 9th AIAA/ISSMO Symposium on Multidisciplinary Analysis and Optimization, Atlanta, GA.

[23]Gaitonde, D. and Shang, J. S., "Accuracy of Flux-Split Algorithms in High-Speed Viscous Flows," *AIAA Journal*, Vol. 31, No. 7, July 1993, pp. 1215–1221.

[24]Josyula, E., Gaitonde, D., and Shang, J., "Nonequilibrium Hypersonic Flow Solutions using the Roe Flux-Difference Split Scheme," *AIAA Paper* 1991-1700, June 1991, Proceedings of the 22^{nd} AIAA Fluid Dynamics, Plasma Dynamics and Lasers Conference, Honolulu, HI.

[25]MacCormack, R. W., "A New Implicit Algorithm for Fluid Flow," *AIAA Paper* 1997-2100, June 1997, Proceedings of the 13^{th} AIAA Computational Fluid Dynamics Conference, Snowmass Village, CO.

[26]Jameson, A., Schmidt, W., and Turkel, E., "Numerical Solution of the Euler Equations by Finite Volume Methods Using Runge-Kutta Time-Stepping Schemes," *AIAA Paper* 1981-1259, June 1981, Proceedings of the 14^{th} AIAA Fluid and Plasma Dynamic Conference, Palo Alto, CA.

[27]Jameson, A., "Multigrid Algorithms for Compressible Flow Calculations," *Princeton University, MAE report 1743*, edited by W. Hackbush and U. Trottenberg, Vol. 1228 of *Lecture Notes in Mathematics*, Springer-Verlag, 1986, pp. 166–201, also in Proceedings of the 2^{nd} European Conference on Multigrid Methods, Cologne, October 1985.

[28]Alonso, J. J., *Parallel Computation of Unsteady and Aeroelastic Flows Using an Implicit Mulrigrid-Driven Algorithm*, Ph d. dissertation, Princeton University, June 1997.

[29]Balay, S., Buschelman, K., Gropp, W. D., Kaushik, D., Knepley, M. G., McInnes, L. C., Smith, B. F., and Zhang, H., "PETSc Web page," 2001, http://www.mcs.anl.gov/petsc.

[30]Balay, S., Buschelman, K., Eijkhout, V., Gropp, W. D., Kaushik, D., Knepley, M. G., McInnes, L. C., Smith, B. F., and Zhang, H., "PETSc Users Manual," Tech. Rep. ANL-95/11 - Revision 2.3.0, Argonne National Laboratory, 2004.

[31]Gill, P. E., Murray, W., and Saunders, M. A., "SNOPT: An SQP Algorithm for Large-Scale Constrained Optimization," *SIAM Journal on Optimization*, Vol. 12, No. 4, Dec. 2002, pp. 979–1006.

[32]Gill, P. E., Murray, W., and Saunders, M. A., "Users Guide for SNOPT (Version 6): A Fortran Package for Large-Scale Nonlinear Programming," Report sol, Dec. 2002, Department of Operations Research, Stanford University, Stanford, CA.

[33]Gaitonde, D. V. and Poggie, J., "Simulation of Magnetogasdynamic Flow Control Techniques," *AIAA Paper* 2000-2326, June 2000, Proceedings of the AIAA Fluids 2000 Conference and Exhibit, Denver, CO.

[34]Hicks, R. M. and Henne, P. A., "Wing Design by Numerical Optimization," *AIAA Journal*, Vol. 15, No. 7, July 1978, pp. 407–412.